Ultrasonics - Sonochemistry 65 (2020) 105062

Contents lists available at ScienceDirect

Ultrasonics - Sonochemistry

journal homepage: www.elsevier.com/locate/ultson

Design a new photocatalyst of sea sediment/titanate to remove cephalexin antibiotic from aqueous media in the presence of sonication/ultraviolet/hydrogen peroxide: Pathway and mechanism for degradation

Fatemeh Tavasol[a], Taybeh Tabatabaie[a,*], Bahman Ramavandi[b,c,*], Fazel Amiri[a]

[a] Department of Environment, Bushehr Branch, Islamic Azad University, Bushehr, Iran
[b] Systems Environmental Health and Energy Research Center, The Persian Gulf Biomedical Sciences Research Institute, Bushehr University of Medical Sciences, Bushehr, Iran
[c] Department of Environmental Health Engineering, Faculty of Health and Nutrition, Bushehr University of Medical Sciences, Bushehr, Iran

ARTICLE INFO

Keywords:
Photocatalyst
Sea sediment
Titanate
Cephalexin
Degradation

ABSTRACT

The aim of the current study was directed to develop a new sea sediment/titanate photocatalyst to remove cephalexin from aqueous media in the presence of ultraviolet (UV) light, hydrogen peroxide (H_2O_2), and ultrasonic waves. The influence of furnace temperature (300, 350, 400, and 500 °C), furnace residence time (1, 2, 3, and 4 h), and ratio of sea sediment: titanium (0–6 v: w) on the physicochemical properties and the cephalexin removal by the sea sediment/titanate photocatalyst was explored. The technique of FTIR, SEM/EDX, XRD, BET, BJH, and Mapping was used to determine the physicochemical properties of the generated photocatalyst. The maximum cephalexin removal (94.71%) was obtained at the furnace temperature of 500 °C, the furnace residence time of 2 h, and the sea sediment: titanium ratio of 1:6 (= 12 mL TiO_2/2 g sea sediment). According to the acquired results, the surface area of the optimized catalyst, namely Cat-500-2-12, was computed to be 52.29 m^2/g. The crystallite size of titanium oxide on the optimum photocatalyst was calculated ~17.68 nm. The FTIR test confirmed the presence of C=C, O-H, C=O, C-S, and C-H functional groups in the photocatalyst. The transformation pathway for the degradation of cephalexin by the developed system was drawn. The present investigation showed that the developed technique (sea sediment/titanate-UV-H_2O_2-ultrasonic) could be used as a promising alternative for attenuating cephalexin from aqueous solutions.

1. Introduction

Nowadays, environmental hazards of antibiotic residues have attracted increasing attention in the world. The release of the domestic, hospital, agriculture (especially animal husbandry), and pharmaceutical wastewaters to the environment have increased antibiotics residue in water bodies [1]. Several antibiotics have been detected in the seawater (1.21 to 51.50 ng/L) and sediments (25.3–32.3 ng/g) of the Persian Gulf [2]. Among the antibiotics, cephalexin has a low biodegradation rate of ~10% and the rest (90%) is excreted in the urine that raises the environmental concerns of antibiotic resistance [3]. Therefore, the continuous input of antibiotics in the environment could result in direct adverse effects on biodiversity and microbial resistance [4]. As a result, removal or destruction of antibiotic pollutants before entering the aquatic environment is a vital issue.

Conventional wastewater treatment methods like flocculation, adsorption, reverse osmosis, and activated sludge processes are designed to remove biodegradable organic matter, microorganism, and dissolved solid [5]. Thus, these techniques cannot effectively remove antibiotic compounds [5]. For this reason, new techniques of advanced oxidation processes (AOPs) have been proposed to remove a variety of antibiotics from aqueous environments. Among AOPs, the ultrasonic- and photo-based methods like NiS-Polypirrol-Fe_3O_4 under sunlight [6], photo- Fenton [7], and magnetic activated carbon [8] were more favorable because they required less reaction time and thus less reactor volume.

In many studies, TiO_2 has been selected as a suitable photocatalyst compared to other semiconductors such as zinc oxide (ZnO), zinc sulfide (ZnS), iron oxide (Fe_2O_3), cadmium sulfide (CdS), cerium dioxide (CeO_2), tungsten trioxide (WO_3), and tin(IV) oxide (SnO_2) [9,10]. The ideal photocatalyst should be chemically and biologically ineffective with light active, light-resistant, inexpensive, non-toxic at the applied

* Corresponding authors at: Department of Environment, Bushehr Branch, Islamic Azad University, Bushehr, Iran (T. Tabatabaie); Systems Environmental Health and Energy Research Center, The Persian Gulf Biomedical Sciences Research Institute, Bushehr University of Medical Sciences, Bushehr, Iran (B. Ramavandi).
E-mail addresses: ttabatabaie@iaubushehr.ac.ir (T. Tabatabaie), b.ramavandi@bpums.ac.ir (B. Ramavandi).

https://doi.org/10.1016/j.ultsonch.2020.105062
Received 4 February 2020; Received in revised form 6 March 2020; Accepted 7 March 2020
Available online 09 March 2020
1350-4177/

quantity, and should be stimulated by visible or UV light [9]. TiO_2 photocatalyst along with UV light has been widely tested to destroy a wide range of drugs [5]. Titanium dioxide can easily be used to modify a wide range of materials to enhance the photocatalytic activity [11,12].

Various studies have reported the applications of photocatalysts in wastewater treatment and research to develop this field is still ongoing. In some studies, TiO_2 contained-photocatalysts were modified with non-metals like nitrogen [13], carbon [14], sulfur [15], boron [16], and also with popular metals such as silver [17], platinum [18], gold [19], and palladium [20] for cephalexin removal. The cephalexin content of the aqueous solution was degraded up to 77% by using Fe-N-Ag-TiO_2 composite during 60 min of light irradiation [7]. One of the drawbacks of composites is the high cost of production and thus the overall cost of cleaning. The treatment cost can be reasonably reduced by the use of waste materials such as offshore sediment during the marsh cracking. Sea sediments (or sludge) in the docks are usually eliminated every several years. Sea sediments (or sludge) contain a variety of minerals (Ti, Mg, Ca, Si, Al, K, Fe, and Zn) that have already been proven to have a photocatalytic/catalytic role [21,22]. Therefore, sea sediments can be used as a photocatalyst in AOPs. Furthermore, the composition of marine sediments is predominantly clay [23], silt, and silica [24], which have previously been tested to purify pollutants. These natural materials (clay, silt, and sand) have been highly considered due to the non-toxic nature, good porosity, low cost, layering morphology, high abundance in the crust, and mechanical stability [25]. Clay can also serve as an efficient support for TiO_2 loading and increase its photocatalytic efficiency [23]. So, likewise clay, marine sediments can be also used as based material for TiO_2 loading and applied in photocatalytic processes.

Another component in the AOPs is the ultrasound system. This system has been used in processes such as sonolysis, sono-ozone, sono-focalist, sono-Fenton, and sonophoto Fenton to treat antibiotics polluted wastewaters [26]. Sonication can produce hydroxyl radicals and play a role in mass transfer [26]. Also, the influence of inorganic oxidants such as H_2O_2 (as a source for radical production) to increase the sono-degradation rate of pharmaceuticals has been proven [27]. The advantages of H_2O_2 over other well-known oxidizers (ozone, persulfate, and periodate) are the convenient storage and oxidation power of OH• by improving the O-O partition with sufficient quantum photon energy [28,29].

For designing and fabricating photocatalysts, the ratio of the components (here, sea sediment to TiO_2), furnace temperature, and furnace residence time should be appropriately selected to provide a suitable surface and functional groups for the photocatalyst, thereby promoting system efficiency. Therefore, the overall objective of this investigation was to optimize the parameters (furnace temperature, furnace time, and sediment: titanate ratio) affecting the fabrication of sea sediment/titanate photocatalyst which has not been generated, optimized, and characterized so far. This photocatalyst was tested to eliminate the cephalexin antibiotic in the system of 'H_2O_2-sonication-UV'. The physicochemical properties of photocatalyst have been characterized for various conditions to make it clearer for further development in the water and wastewater industry, especially for the removal of emerging pollutants.

2. Experimental section

2.1. Materials and solutions

Deionized water has been used to provide solutions. Tetrapropyl ortho-titanate was purchased from Merck Company. Hydrogen peroxide (H_2O_2) with a purity of 35% was supplied by Kimia Exir (Iran). Ethanol (96%) was provided by Khorasan Distillery Company, Iran. NaOH and HCl were prepared from Kimia Mavad, Iran. The powder of cephalexin (99.8% purity) was supplied from Dana Pharmaceuticals Limited, Iran and used without any processing.

2.2. Preparation of cephalexin stock solution and its COD

The precise amount of 0.02 g of cephalexin (with chemical formula $C_{16}H_{17}N_3O_4S{\cdot}H_2O$ and molecular weight of 347.39 g/mol) was weighed with a digital weighing scale (Ohaus Pioneer) and delivered to a volume of 20 mL to give a cephalexin stock solution with a concentration of 1000 mg/L. The main solution was provided daily because of the possible volatility of the drug. The COD value of the cephalexin contaminant (concentration: 100 mg/L) was measured to be 208 ± 3 mg/L.

2.3. Reactor specification for antibiotic removal tests

A 3-L water bath sonication device (Sonica brand, Model 2200 EP manufactured by SOLTEC, Italy) with a frequency of 40 kHz was used as a source of ultrasonic waves. The stainless-steel reactor used in this study was a cylinder (high: 24 cm, diameter: 4.1 cm, and volume: 460 mL) equipped with a UVC lamp (15 w, Charge Jiang UV) in a glass tube in the middle. The distance of the quartz lamp body to the inner wall of the reactor was 1.5 cm. Due to the low depth of the sonication device, the reactor was diagonally (not horizontally) mounted in the device. The working volume of antibiotic solution in the reactor was set to 150 mL to receive ultrasound waves when it placed in the device. The water temperature in the ultrasonic device was also kept constant during the reaction by a constant flow rate of tap water through the inlet and outlet valve of the device.

2.4. Sea sediment preparation

The sediments were collected from the shipping pier of Jofreh in Bushehr (Iran). The sediments were first placed in the oven at 105 °C for 24 h to dry completely. The dried sediments were then milled and passed through a sieve with mesh number 40. Some of the important compounds and heavy metals in the raw sediment used for photocatalyst generation are listed in Tables 1 and 2.

2.5. Fabrication of sea sediment/titanate photocatalyst

In this study, the sol–gel method was applied for photocatalyst preparation [30,31]. Two solutions were used as follow:

Solution A: 4 mL of titanium propoxide was added dropwise to 2 mL of ethanol and stirred at room temperature for 30 min.

Solution B: 0.4 mL of nitric acid (HNO_3) and 2 mL of deionized distilled water were added to 17 mL of ethanol.

Solution B was added dropwise (3 mL/min) to Solution A and stirred for 1 h to give clear sol. The exact amount of 2 g of sea sediment was added to the transparent sol and stirred for 30 min. Afterward, it was

Table 1
Specifications of the raw sediment sample used for photocatalyst preparation.

pH	Cl%	Organic matter	MgO%	CaO%	SO_3%	Al_2O_3%	Na_2O%	K_2O%	Fe_2O_3%
7.30	1.46	3.6	2	49	0.19	13.70	3.92	0.72	7.5

Table 2
Metal content in raw sediment sample used for photocatalyst preparation by ICP-OES method and their corresponding wavelengths (nm).

Element	Wavelength (nm)	Concentration (μg/g)
Al	396.152	7479.80
As	188.980	4.97
B	249.772	27.62
Ba	455.403	86.18
Be	313.107	0.08
Ca	318.127	201063.81
Ce	418.659	7.41
Co	228.615	1.87
Cr	267.716	46.20
Cu	324.754	5.03
Fe	259.940	5160.66
K	766.491	1998.60
La	408.671	2.87
Li	670.783	2.99
Mg	280.270	9657.36
Mn	260.568	128.23
Na	568.821	4479.04
Ni	231.604	8.59
P	213.618	203.52
Pb	220.353	0.91
S	181.972	114.06
Sc	335.372	1.04
Sr	460.733	1205.00
Ti	334.188	1124.69
V	292.401	14.59
Y	360.074	2.61
Zn	334.502	4.07
Zr	349.619	2.19

incubated at room temperature (without stirring) for 24 h. The final solution was dried at 80 °C for 3 to 6 h. Then, the dried solution was calcined at 300 °C for 3 h. Thus, the catalyst was obtained at a temperature of 300 °C. The same steps were repeated for the preparation of photocatalyst at furnace temperatures of 350, 400, and 500 °C for 3 h (as furnace residence time). After cooling, the catalyst samples were powdered and kept in containers for cephalexin removal experiments.

2.6. Steps to optimize photocatalyst production

The optimization of the sea sediment/titanate photocatalyst production was done in three steps as follows:

Step 1- Furnace temperature: To obtain the optimal value of the furnace temperature, the sea sediment/titanate photocatalyst were stayed in the furnace for 3 h at different temperatures of 300, 350, 400, and 500 °C, the titanate: sea sediment ratio of 4 mL: 2 g, the catalyst dose 0.225 g/150 mL, and cephalexin concentration of 100 mg/L. The pH of the solution was also adjusted to 6.8 ± 0.2.

Step 2- Furnace duration time: To optimize this factor, the variable was furnace residence time (1, 2, 3, and 4 h) and other items were fixed like the previous step.

Step 3- The ratio of titanate to sea sediment: After determining the optimum values for furnace duration and furnace temperature, experiments were continued to optimize the ratio of titanate to sea sediment (0, 2, 4, 6, 8, and 12 mL of titanate per 2 g of sea sediment). For this stage, other items were considered like those presented for Steps 2& 3.

Details for test conditions of the above steps are presented in Table 3.

2.7. Measurements

The field emission scanning electron microscope (FESEM) images of photocatalyst samples were provided using the SIGMA VP model of the German Zeiss Electron Microscope Scanner. The samples were subjected to a high vacuum with a thin layer of gold for electrical conductivity in a sputtering system. Measurements of the specific surface area were done using an automated BET Surface- Micrometric (USA) model ASAP 2020- by measuring nitrogen uptake at 77 K. Functional groups were analyzed using Fourier transmission infrared (FTIR, Bruker-Germany Tensor Device Model II) in the range of 400 to 4000 cm^{-1}. The generated photocatalyst samples were characterized by X-ray diffraction technique (XRD, D8 advance X-ray diffractometer) with Cu Kα to describe the crystal structure, operated at 40 kV and 40 mA. The chemical composition was evaluated simultaneously by EDX- mapping experiments using the Oxford Instrument Company (UK). The COD measurement was performed using HACH spectrophotometer DR6000 at λ = 620 nm after the removal of the interferers. The concentration of metals in sea sediment was analyzed by the ICP method using ICP-OES 730-ES, Varian.

Table 3
Reaction conditions for optimization of effective parameters for the construction of sea sediment/titanate photocatalyst for cephalexin removal (pollutant concentration: 100 mg/L, sonication time: 100 min, catalyst dose: 1.5 g/L).

Run	Furnace temperature (°C)	Furnace residence time (h)	Ratio of mL TiO_2: 2 g sediment	Catalyst name
Effect of furnace temperature	300 **350** 400 500	3	4	Cat-500-3-4
Effect of furnace residence time	500	1 **2** 3 4	4	Cat-500-2-4
Effect of titanate to sediment ratio	500	2	0 **2** 4 6 8 12	Cat-500-2-12

Bolded numbers indicate the optimal amount of items.

3. Results and discussion

3.1. Characterizations of the photocatalyst samples

3.1.1. FTIR patterns

The FTIR spectra of Cat-500-3-4, Cat-500-2-4, Cat-500-2-12 photocatalysts are shown in Fig. 1 A, B, and C, respectively. According to the figures, five peaks are visible at wavelengths less than 1600 cm^{-1}. The very small peak visible at a wavenumber of ~2320 cm^{-1} is related to the CO_2 gas remaining in the sampling chamber. The widespread peak in the wavenumber of 1418 cm^{-1} corresponds to the flexural vibration of the C-H bond [32]. The tensile vibration waves of the C=C groups of the aromatic rings [33] may also interfere with the peak of the C-H bonds in this wavenumber, causing the peak to be widened. Visible peaks at the wavenumbers of 1047 cm^{-1}, 871 cm^{-1}, and 711 cm^{-1} belong to the C-N bond vibration [34], the O-H bond vibration [35], and tensile vibration of C-S bonds, respectively. It is observed that these peaks are intensified after reaction with cephalexin, which may indicate an increase in the amount of the bonds after the reaction of the contaminant with the photocatalyst surface. Also, the visible peak at wavelengths less than 800 cm^{-1} is related to metal oxide bonds like titanate [36]. The intensity of this peak also decreased after reacting with cephalexin. It may reflect the adsorption of the pollutant onto the catalyst surface and/or the reaction between the C=O groups with the metals present in the sediment. This hypothesis can be substantiated by the lack of observation of C=O groups in the wavenumber around 1700 cm^{-1} [37].

In Fig. 1C (Cat-500-2-12 photocatalyst), in addition to the peaks observed in the previous spectra, two weak peaks were also visible at

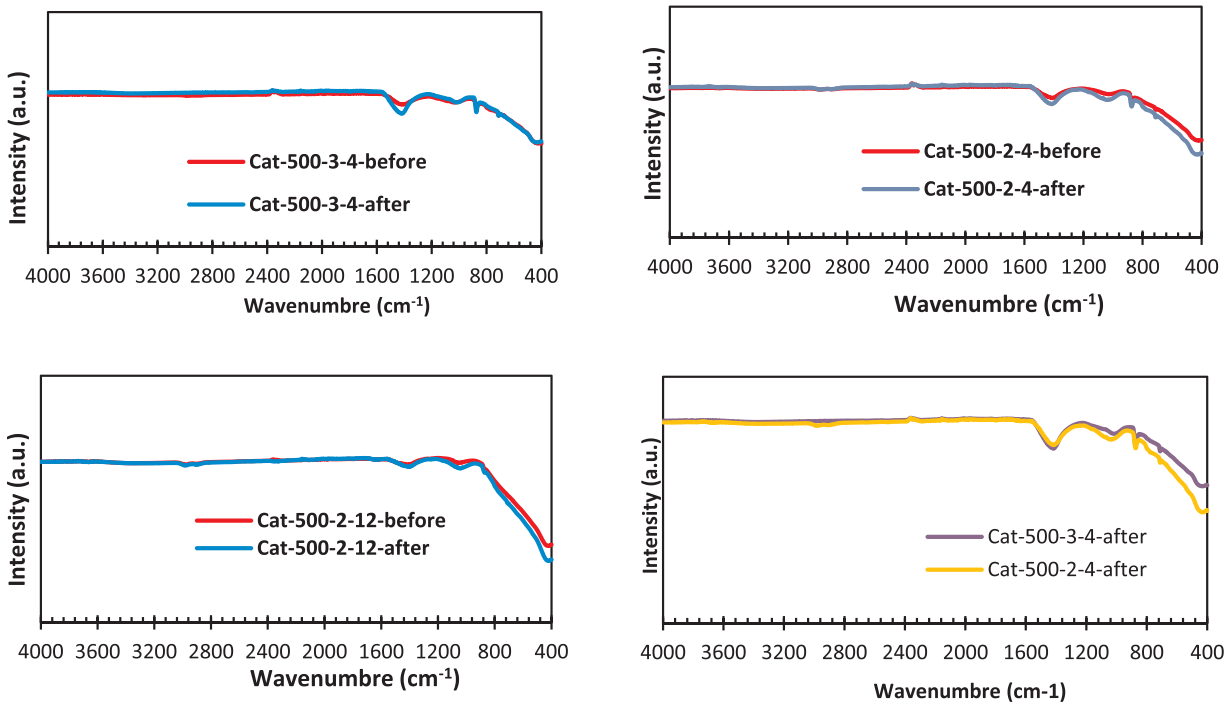

Fig. 1. FTIR spectra for the photocatalysts prepared in this study for before and after cephalexin removal.

the wavenumbers of about 2980 cm^{-1} and 2890 cm^{-1}, which correspond to the symmetric and asymmetric tensile vibrations of C-H bonds in the system, respectively [38]. The spectra also show that the wavenumbers decreased after the reaction, confirming the successful oxidation of cephalexin on the catalyst surface.

3.1.2. XRD patterns

The XRD spectra of Cat-500-3-4, Cat-500-2-4, and Cat-500-2-12 photocatalysts before and after the sono-photocatalytic reaction is illustrated in Fig. 2A, B, and C, respectively. The two XRD spectrum before and after cephalexin removal had approximately identical peaks. By matching these two spectra to the reference spectra, the calcite compounds (Reference code: 01-086-2334), silicon oxide (Reference code: 01-077-1060), and titanium oxide (Reference code: 01-075-1582) at the catalyst structure is identifiable. A comparison of two XRD spectrum before and after cephalexin removal revealed that the spectral peak intensities have been decreased. This decrease in crystal peak intensity after reaction with cephalexin may be due to the formation of a layer of the contaminant (or intermediate products of its removal) on the catalyst surface.

In Fig. 2C, the peaks for Cat-500-2-12 are wider than other studied photocatalysts that indicate a decrease in the crystallite size of the titanate crystals. It is also observed that the saturation of the contaminant (cephalexin) on the catalyst surface reduces the intensity of the crystalline peaks. This confirms the successful reaction of organic (contaminant) molecules with the crystalline surface of the sea sediment catalyst.

3.1.3. SEM/EDX patterns

The surface morphology of the titanate/sea sediment samples before and after the sono-photocatalytic reaction is depicted in Fig. 3. The figures show that the surfaces of the photocatalysts (both reacted and unreacted) are similar and have particles with different sizes and white color. White particles may be due to the interaction of inherent elements in sea sediment such as Ti, Cl, Mg, Ca, S, Al, Na, K, Fe, and Zn with TiO_2 crystalline particles. Cracks are also visible on the catalyst surfaces.

Elemental analysis and mapping results for the Cat-500-3-4 sample before the reaction with cephalexin are provided in Fig. 4A, B. The figure has been proven that metals such as zinc, magnesium, copper, and aluminum have a catalytic role in the removal of cephalexin. The XRD test also confirms the presence of titanium in the photocatalyst. The results of the elemental surface analysis of the Cat-500-3-4 photocatalyst after the reaction with cephalexin are also shown in Fig. 4C, D. In addition to metals present in the sea sediment/titanium oxide, the percentage of sulfur and oxygen in the reacted catalyst has been significantly increased and at the same time, the percentage of titanium element has been decreased. These observations confirm that the catalyst surface is covered by a layer of cephalexin or its intermediate products. Concludingly, the acquired findings confirm the successful reaction of cephalexin with the photocatalyst surface.

According to Fig. 4E, F, high levels of calcium, chlorine, and metals such as copper, zinc, and titanium were demonstrated for Cat-500-2-4 (before reacting with cephalexin), which was previously confirmed by XRD test. Also, the amount of carbon and sulfur in the elemental analysis results was low because this is a pre-reacted sample. The results of the elemental and surface analysis of the Cat-500-2-4 sample after reaction with cephalexin are prepared in Fig. 4G, H. After the reaction of the Cat-500-2-4 photocatalyst with cephalexin, the percentage of carbon, sulfur, nitrogen, and oxygen in the sample increased significantly and the amount of titanium and other metals decreased. This indicates that the catalyst surface is covered by cephalexin molecules or its intermediate products.

Fig. 4I- L has been shown the elemental analysis results of the Cat-500-2-12 sample before and after the reaction with cephalexin. As shown in Fig. 4I, J, the Cat-500-2-12 sample (before reaction with cephalexin) contains various metals, chlorine, sodium, and titanium. The presence of TiO_2 in the system was also confirmed by the XRD test. In Fig. 4k, L, the increase in the percentage of oxygen, carbon, sulfur, and nitrogen in the catalyst structure, along with the decrease in titanium percentage, indicate the removal of cephalexin.

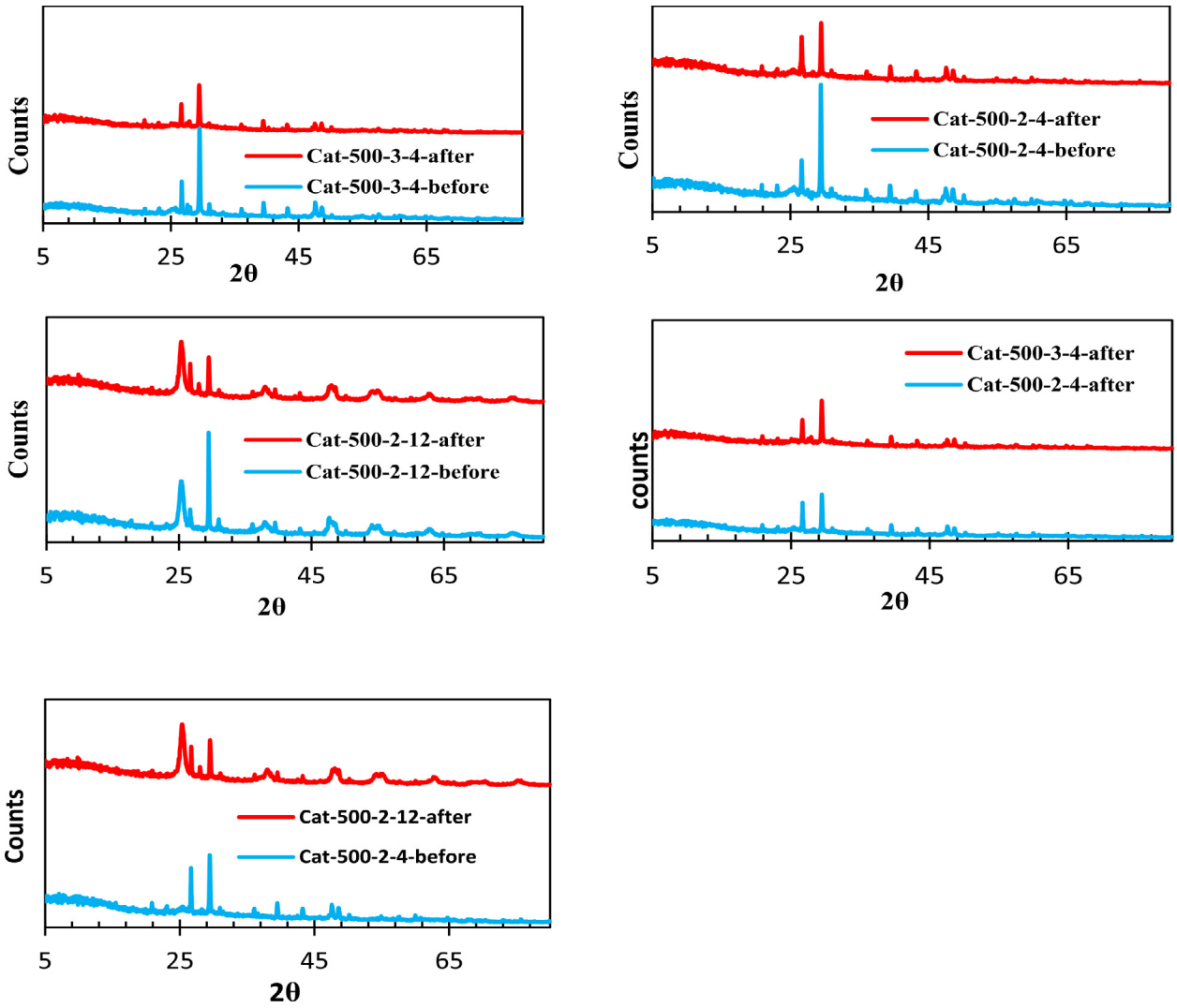

Fig. 2. XRD for photocatalysts prepared in this study before and after cephalexin removal.

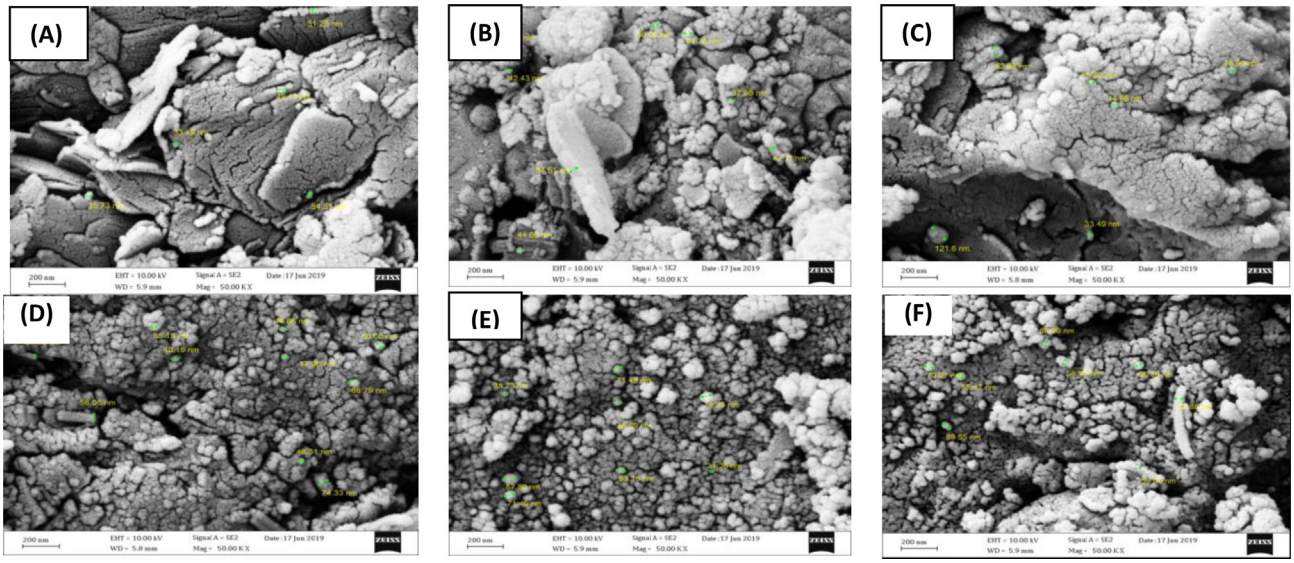

Fig. 3. SEM for photocatalysts prepared (A) Cat-500-3-4 before reaction, (B) Cat-500-3-4 after reaction, (C) Cat-500-2-4 before reaction, (D) Cat-500-2-4 after the reaction, (E) Cat-500-2-12 before the reaction, and (F) Cat-500-2-12 after the reaction.

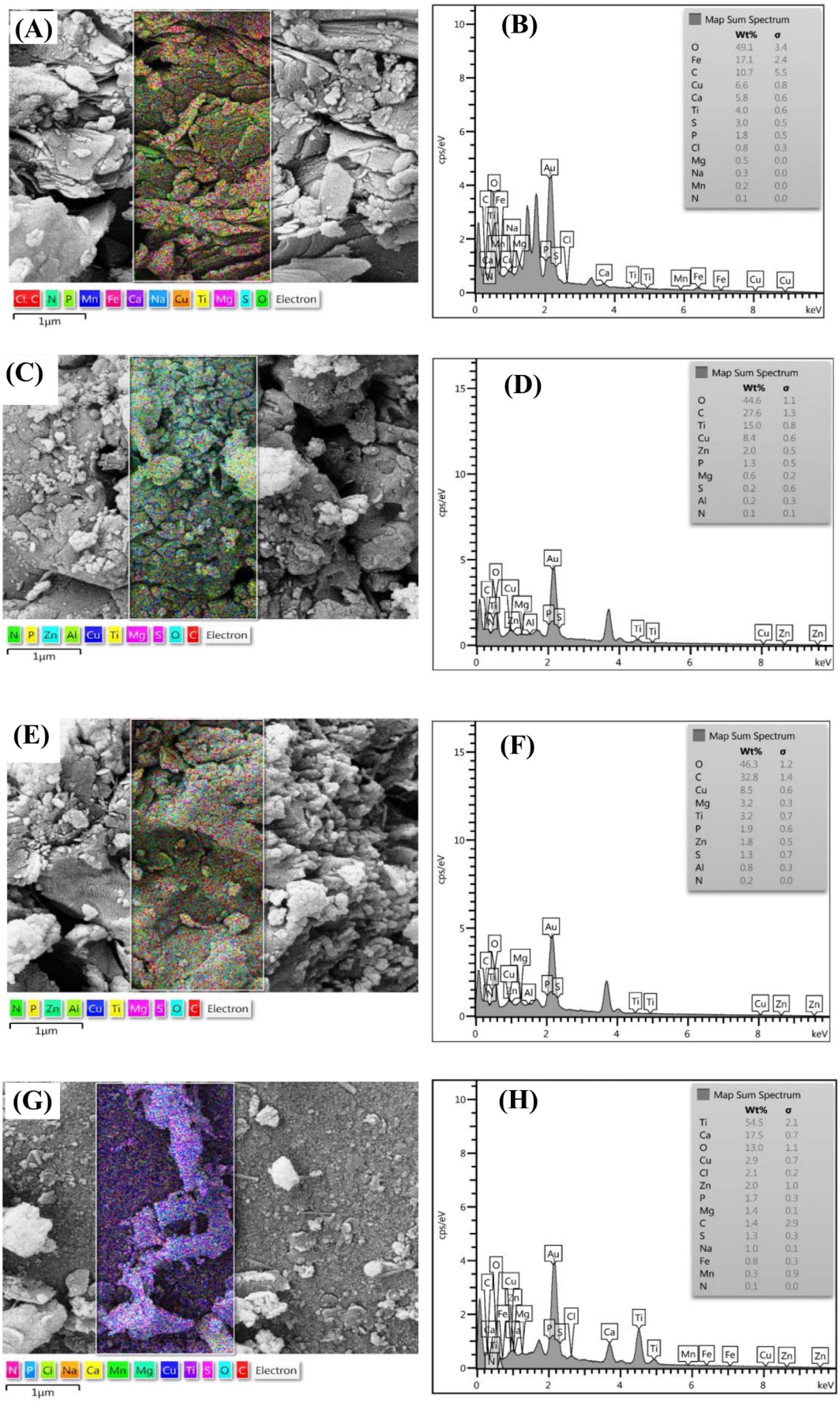

Fig. 4. Mapping and EDX for the photocatalysts prepared in this study [(A, B- before, C, D-after for Cat-500-3-4; (E, F-before, G, H-after for Cat-500-2-4), and (I, J-before, K, L-after for Cat-500-2-12].

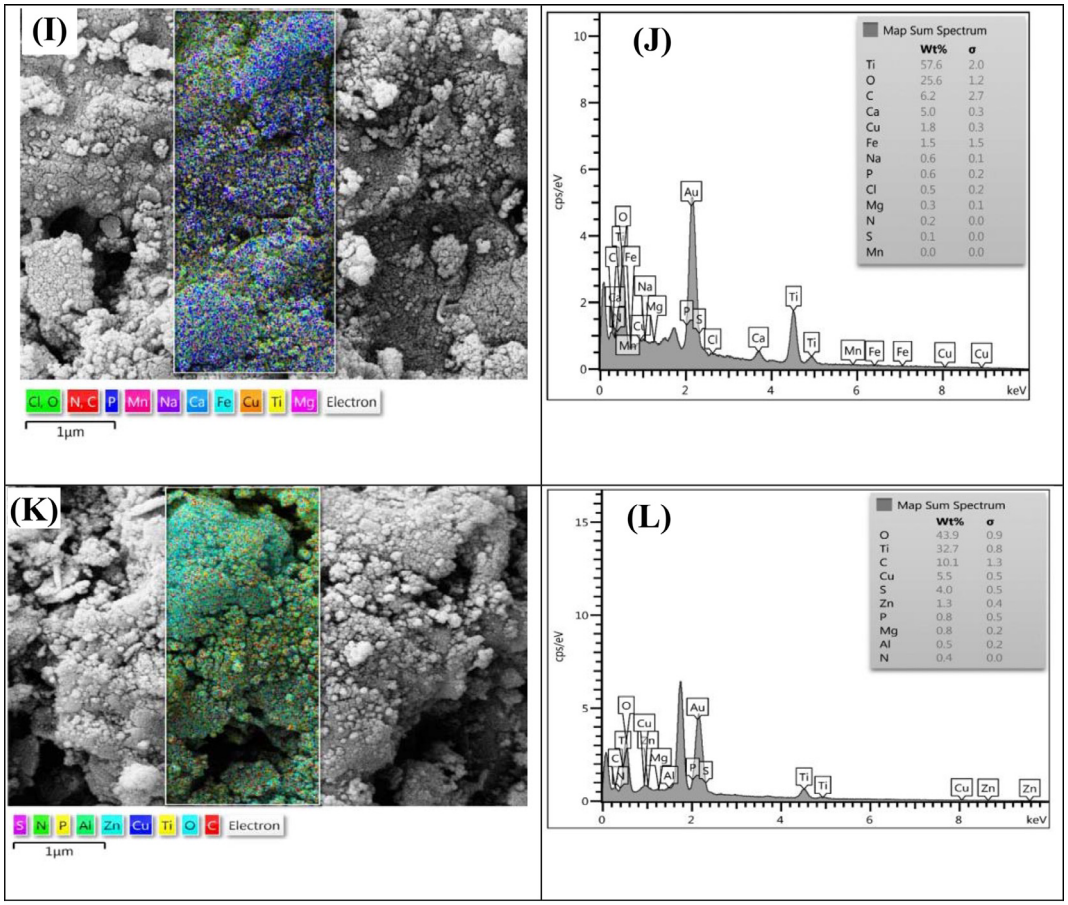

Fig. 4. (*continued*)

3.1.4. BET patterns

Table 4 shows the physical properties of the optimized photocatalyst (in terms of furnace temperature, furnace duration, and titanate loading rates) before and after sono-photocatalytic reaction based on the BET and BJH model.

The photocatalyst surface is an important parameter in antibiotic degradation reactions in heterogeneous systems because the amount of surface area available for the reaction determines the operational efficiency. This is especially important when considering large-scale and industrial applications. According to Table 4, the BET surface area before the sono-photocatalytic test for three catalysts of Cat-500-3-4, Cat-500-2-4, and Cat-500-2-12 was obtained 42.04 m^2/g, 46.07 m^2/g, and 52.29, m^2/g, respectively. As it can be seen, the Cat-500-2-12 photocatalyst has the highest BET value which can be attributed to the strong reaction between Mn and Mo [39] and other impurities including partial dissolution and conversion from hematite phase particularly in meso- and macro- porous $Fe(OH)_3/FeOOH$ [40] and elements (according to ICP results, see Table 2). The specific surface area after the sono-photocatalytic test for Cat-500-3-4, Cat-500-2-4, and Cat-500-2-12 has been obtained 41.18 m^2/g, 52.22 m^2/g, 58.91 m^2/g, respectively. As it can be seen, the sea sediment catalyst has the highest BET level for the furnace temperature of 500 °C, 2 h' furnace duration, and 12 mL titanate (Cat-500-2-12) after the sono-catalytic reaction. Besides, after the reaction, the surface area has increased for most photocatalysts, which may be due to the attack of hydroxyl radicals resulting in the formation of new pores or expansion of the previous ones [41].

High active surface area is useful for adsorption and reaction with contaminants. According to Table 4, the external surface area for the catalysts Cat-500-3-4, Cat-500-2-4, and Cat-500-2-12 before the reaction was 38.86 m^2/g, 47.81 m^2/g, and 51.07 m^2/g, respectively that can be attributed to the increased amount of titanate [42]. However, the micropore surface area for the fresh Cat-500-3-4 and Cat-500-2-12 catalyst has increased after the reaction with the antibiotic. This can be due to the negative volume of the micropores or the external surface being larger than the entire surface.

Fig. 5 shows the adsorption-desorption isotherm of nitrogen gas of catalysts prepared from sea sediment. In all figures, the adsorption-desorption curve is of type IV Langmuir adsorption, which is the characteristic of usual mesoporous materials. In other words, there is a large hysteresis loop (type H1) at high relative pressures where the

Table 4
Some of the most important characteristics of photocatalyst prepared from sea sediment for cephalexin removal.

External surface area (m^2/g)		Micropore area (m^2/g)		Pore size (nm)		Pore volume (cm^3/g)		BET surface area (m^2/g)		Catalyst
Reacted	Fresh	Reacted	Fresh	Reacted	Fresh	Reacted	Fresh	Reacted	Fresh	
41.10	38.86	0.08	3.17	9.54	11.22	−0.0005	0.001	41.18	42.04	Cat-500-3-4
51.99	47.81	0.22	*	7.13	10.65	−0.0005	−0.001	52.22	46.07	Cat-500-2-4
59.89	51.07	*	1.21	7.97	8.25	−0.001	0.00001	58.91	52.29	Cat-500-2-12

* The micropore area is not reported because either the micropore volume is negative or the calculated external surface area is larger than the total surface area.

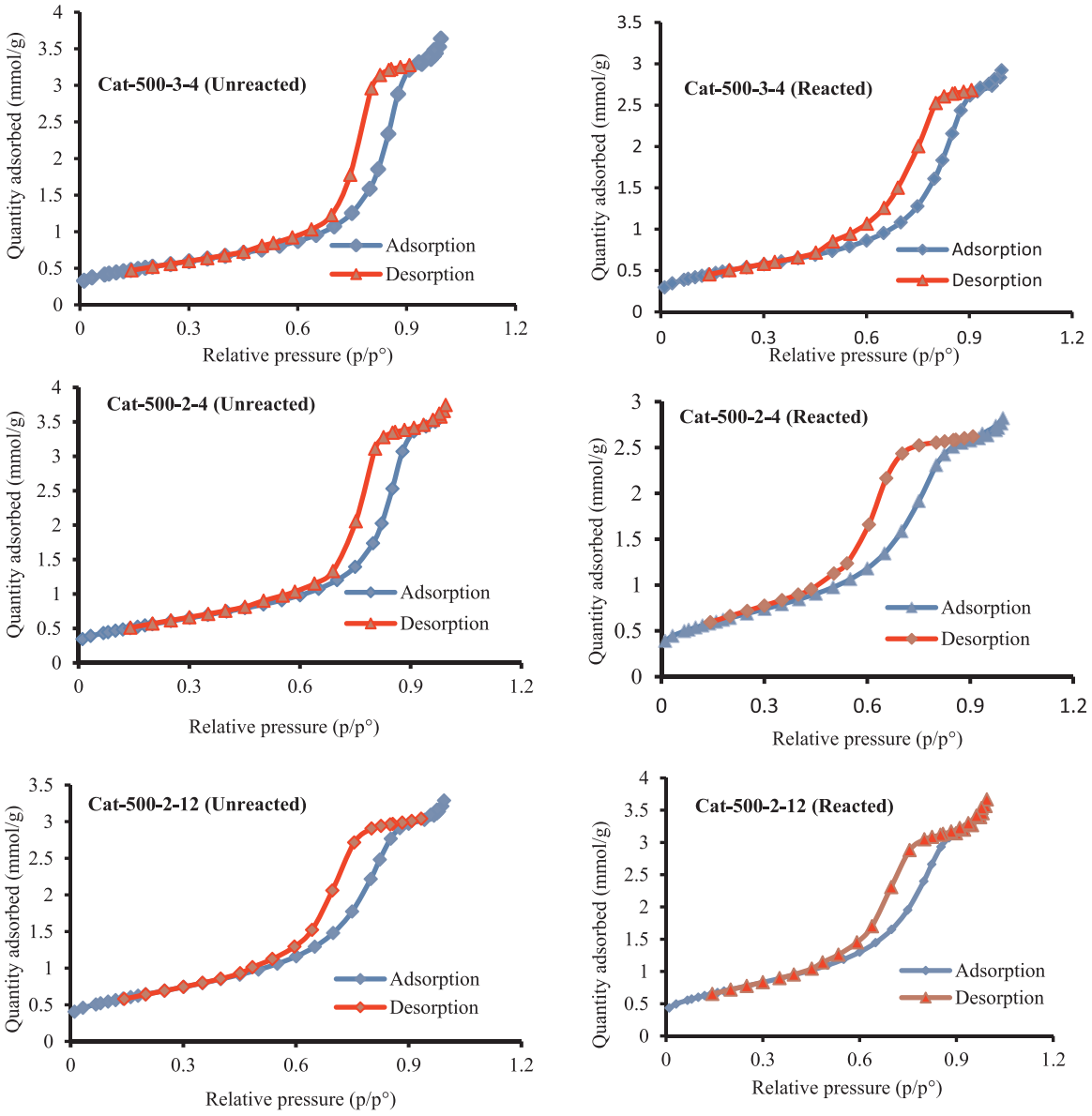

Fig. 5. Adsorption and desorption isotherms for photocatalysts prepared in this study.

agglomerated or spherical particles are arranged in a cylindrical shape with a large size and easily interconnected. On the other hand, the photocatalysts samples belong to Type A which represents cylindrical cavities that are open at both ends (according to the BET model and the IUPAC classification) [43]. At the relative pressure of $p/p^0 = 0.5$, it can be seen that the mesopore distribution is high and therefore, the high desorption rate occurs faster due to the openness of the pore (Fig. 5). The adsorption capacity increased for $p/p^0 > 0.5$ due to the multilayer adsorption of N_2 molecules on the inner surface of the mesopores materials. As the relative pressure increases to 0.6, the adsorption capacity gradually increases and then the adsorption value changes drastically due to the N_2 capillary density.

Based on Table 4, the pore size parameter decreased after reacting with the antibiotic, which indicates the blocking of the photocatalytic surface by cephalexin sequestration. Further, TiO_2 particles may settle within the interior cavities in the photocatalysts after reaction [30]. Based on the acquired data in Table 4, the pore size diameter for all catalysts is within the range of 2–20 nm. This confirms the mesoporous nature of the studied materials. The reason for the size values obtained for the photocatalysts could be due to differences in MO bonds (M: iron or aluminum or metal compounds present in sea sediment, O: oxygen) because the bond lengths of Fe-O and Al-O are 0.197 nm and 0.167 nm, respectively [44].

According to Fig. 5 and BET specifications in Table 4, the sea sediment loaded with 12 mL of titanate (Cat-500-2-12) is a high surface and mesoporous material. A high surface area is one of the main parameters affecting the catalytic activity of a material. This is due to the availability of more sites to react with the target contaminant. Therefore, optimization of the method for fabricating the photocatalyst is one of the main points of interest for researchers [43].

3.2. Influence of physical factors for manufacturing photocatalysts on the cephalexin removal

3.2.1. Influence of furnace temperature

The results of cephalexin removal by the photocatalyst prepared at different furnace temperatures (300, 350, 400, and 500 °C) are presented in Fig. 6. As depicted in this figure, the efficiency is increased with the increase of temperature up to 500 °C. The highest percentage of cephalexin removal (80.76%) was obtained at 500 °C. The

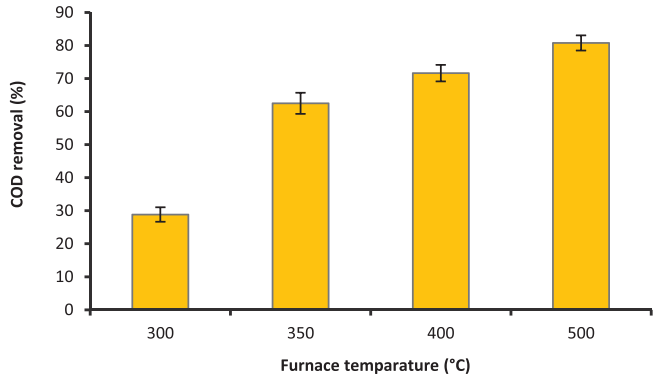

Fig. 6. Percentage of cephalexin removal by sea sediment photocatalyst prepared at different temperatures after sonication (pH: 6.8 ± 0.2, H_2O_2: 0.7 mL, sonication time: 100 min, catalyst dose: 0.225 g per 150 mL, UVC intensity: 15 W).

calcination temperature of each catalyst has a direct effect on the crystallization and its photovoltaic activity [45]. Increasing temperature affects the deployment and arrangement of titanium dioxide crystals [46]. This factor, in turn, affects the increase in specific surface area and thus the photocatalytic efficiency. Researchers have reported that the increase in the removal efficiency by increasing the furnace temperature (in catalyst production) could be due to the expansion of the catalyst crystalline network and the rebuilding of bands by the formation of rutile nuclei and crystalline growth [23,46]. Calcination has not been tested at temperatures above 500 °C because at 600 °C the rutile TiO_2 phase is predominant and photovoltaic activity is reduced [23].

The catalyst preparation method is the main factor affecting its chemical and physical properties. Generally, high temperatures (> 449.85 °C) are required to form a regular crystalline structure and above this temperature will in particular decrease the TiO_2 surface area and decrease the effective groups' surface area. Catalyst preparation at high temperatures also increases particle distribution and thermal stability when used in water or wastewater [47].

3.2.2. Influence of the furnace residence time

Fig. 7 shows the cephalexin removal by developed photocatalyst prepared at different furnace residence time (1, 2, 3, and 4 h). As can be seen, the efficiency first increased from 1 h to 2 h and then approximately remained unchanged. The removal rate for 4 h furnace duration was 83.65%, which is slightly different from those obtained for 2 h (82.69%). Thus, the optimal residence time of 2 h (Cat-500-2-4) was considered to save energy and reduce costs [48].

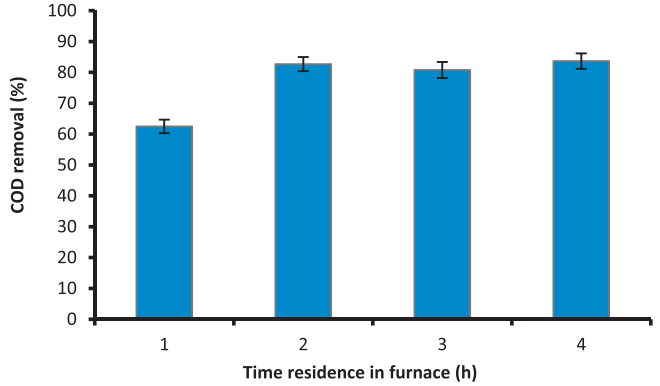

Fig. 7. Percentage of cephalexin removal by sea sediment photocatalyst prepared at 500 °C at different times furnace (pH: 6.8 ± 0.2, H_2O_2: 0.7 mL, sonication time: 100 min, catalyst dose: 0.225 g per 150 mL, UVC intensity: 15 W).

Based on the results of the FTIR test in Fig. 1D for Cat-500-2-4 and Cat-500-3-4 after the photocatalytic reaction, the reduction in wavenumbers of Cat-500-2-4 is greater than Cat-500-3-4. This indicates that the effectiveness of Cat-500-2-4 photocatalyst for the degradation of cephalexin. This result confirms the previous test. According to the XRD test for reacted Cat-500-2-4 and Cat-500-3-4 (Fig. 2D), the peak intensities of the crystalline structures corresponding to sample with 2 h residence time in the furnace is less than 3 h one. Therefore, it is implied that the Cat-500-2-4 catalyst has more potential for catalyzing cephalexin in the sono-photocatalytic reaction.

An important factor in the preparation of photocatalyst is the length of calcination time. The optimum calcination time was obtained 2 h and calcination at or below this time resulted in lower photocatalytic activity. Less activity in very short calcination time (here, 1 h) may be due to incomplete conversion of metal salts to the corresponding oxide in marine sediment and for periods longer than 2 h due to a high degree of particle aggregation [48].

3.2.3. Influence of titanium to sea sediment ratio

The acquired results of antibiotic removal by the photocatalyst prepared with different 'titanate to sea sediment' ratios are illustrated in Fig. 8. As the titanate content increases, the removal efficiency of the target contaminant increases, with the maximum efficiency (94.71%) at a ratio of 12 mL titanate to 2 g of sea sediment (Cat-500-2-12). By increasing titanate, the outer surface area of the photocatalyst particles can be increased. According to Table 4, the specific surface area for Cat-500-2-12 (51.07 m2/g) was higher than the other two catalysts, which can be attributed to the increase in titanate content of the catalysts [30]. Modification of the surface of clay grains with titanate has been also shown to have a significant effect on photovoltaic activity due to increased surface area [23]. In addition to increasing the active photovoltaic sites, the increase of titanate also strengthens the catalyst against shear forces [30]. The sea sediment catalyst modified with 12 mL titanate (Cat-500-2-12) has a higher efficiency in cephalexin removal than the 4 mL modified type (Cat-500-2-4) under similar conditions. Therefore, increasing the titanium content of the photocatalyst results in a higher specific surface area and ultimately oxidation efficiency. This finding is in good agreement with the study on the TiO_2/namontmorillonite nanocomposite [30].

In this investigation, the best removal (94.71%) was attained by loading 12 mL of titanate onto the sea sediment (Cat-500-2-12) when the titanate was reduced to 6 mL (Cat-500-2-6), the removal rate was significantly reduced (73.55%) due to the decrease in effective catalytic sites. Increasing the titanate content in the photocatalyst contributes to the catalytic process and results in the formation of more OH radicals. Similar results have been reported by other researchers [49,50].

Fig. 2E shows the comparison of the XRD results for Cat-500-2-4 and Cat-500-2-12 photocatalysts after being used in the cephalexin removal.

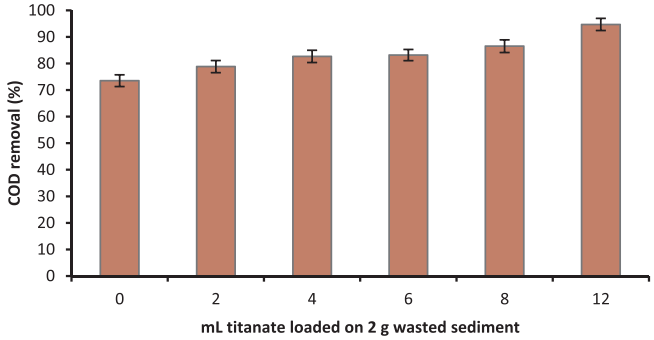

Fig. 8. Percentage of cephalexin removal by photocatalyst prepared from sea sediment at 500 °C for 2 h and loading different amounts of titanate (pH: 6.8 ± 0.2, H_2O_2: 0.7 mL, sonication time: 100 min, catalyst dose: 0.225 g per 150 mL, UVC intensity: 15 W).

As illustrated in Fig. 2E, peaks are less intense in samples containing 4 mL of titanate (Cat-500-2-4). Also, broadening peaks in the presence of higher amounts of titanate means that the crystallite size of the titanium oxide is reduced. To calculate the crystallite size (D, nm), the Scherrer equation was used.

$$D = K\lambda / B\cos(\theta) \quad (1)$$

where λ is the x-ray wavelength used (here, 1.54 angstrom), K is the shape factor (approximately 0.9), B is the peak width at half-height, and θ is the peak location. The crystallite size of the titanium oxide for samples containing 4 mL and 12 mL of titanate was calculated to be 45.89 nm and 17.68 nm, respectively. The decrease in the photocatalytic behavior of the smaller nanoparticles can be due to the increased level of recombination of the electrons and cavities and the produced photonic surface [49].

On the other hand, at higher titanate loads, the cephalexin removal through adsorption is more pronounced. The presence of titanate on the surface of the sediments likely changes the polarity of TiO_2, such as the decrease in zero-point charges content and thus, higher cephalexin removal [51].

In photocatalytic degradation, the stability and effectiveness of the catalyst in the removal of contaminants depending on the total pores and surface area of the catalyst [52]. As the size of the support surface decreases, the surface area increases, leading to an increase in the number of active sites, thereby promoting photovoltaic activity [23]. In this study, the crystalline size of the Cat-500-2-12 particle was about 17.68 nm and provides more surface area for catalytic activity than Cat-500-2-4 (crystalline size: 45.89 nm). The Cat-500-2-12 catalyst was, therefore, most effective in removing cephalexin.

The optimal loading of titanate for degradation of cephalexin is greatly affected by the preparation method [48]. For example, the sea sediment/TiO_2 catalyst prepared using the sol-gel method has the highest activity for the degradation of cephalexin under the UV lamp at 12 mL of titanate. On the other hand, the titanate loading on the sea sediment was performed in acidic medium (nitric acid) resulted in the catalyst with a higher specific surface. This is consistent with a study on the specific surface enhancement of TiO_2/montmorillonite nanocomposites prepared at pH = 1.0 because at the low pH the solubility of the ions is higher [42]. Therefore, the pores volume and the photonic ability of the catalyst samples increased in acidic medium.

3.3. Cephalexin degradation pathway

Products and intermediates derived from the decomposition of cephalexin by UV light, ultrasonic wave, and H_2O_2 oxidizer in the presence of Cat-500-2-12 photocatalyst were investigated by GC-Mass (Fig. 9a). It is expected that hydroxyl radicals, formed by UV irradiation to hydrogen peroxide, are involved in the degradation of cephalexin [53]. Also, hydroxyl radicals created by ultrasonic waves play a role in pollutant degradation. The molecular structures were analyzed and plotted based on the molecular weight of *m/z* obtained from the mass spectrum by ChemDraw software [54]. Proposed structures and degradation pathways caused by the loss of methyl groups, carboxyl groups, hydroxyl groups, alkyl groups, and oxygen atoms are shown in Fig. 9b [53]. Structures with molecular weights of 222.08 g/mol and 318.25 g/mol have been previously reported by Gawande et al. [55]. Antonin et al. [53] also proposed molecular weights of 386.67 g/mol and 326.88 g/mol. Besides, molecules with weights of 280.13 g/mol and 138.14 g/mol have been reported by researchers [7,54] as end products of cephalexin degradation.

3.4. Proposed mechanism for cephalexin degradation

Fig. 10 illustrates the proposed mechanism of degradation of cephalexin by the UV/ultrasound/H_2O_2 system at near-neutral pH. In fact, at optimum pH, iron and other metals such as Ti, Cl, Mg, Ca, S, Al, Na, K, Fe, and Zn in the sea sedimentation/titanate have been reacted with the antibiotic. Thus, the synergistic effect of photo-Fentonic, photocatalyst, and ultrasound has produced more hydroxyl radicals. Abundant hydroxyl radicals (based on Eqs. (2)–(11) are produced by photocatalysis and UV/ultrasound processes, which ultimately results in a synergistic effect and improves the cephalexin degradation efficiency. During these processes, the coupling of electrons and cavities at the TiO_2 surface is prevented. Thus, the production of ferrous and other ions present in sea sediment to a lesser capacity is promoted by the TiO_2-stimulated photoelectron (due to UV radiation) [50]

$$H_2O \xrightarrow{UV} OH^{\cdot} + H^{\cdot} \quad (2)$$

$$C_{16}H_{17}N_3O_4S{\cdot}H_2O + OH^{\bullet} \rightarrow CO_2 + H_2O + \text{Intermediates} \quad (3)$$

$$TiO_2(h^+) + Y \rightarrow TiO_2 + Y^+ \quad (4)$$

$$TiO_2(h^+) + H_2O \rightarrow TiO_2 + OH^{\bullet} + H^+ \quad (5)$$

$$TiO_2(e^-) + O_2 \rightarrow TiO_2 + O^{2-} \quad (6)$$

$$TiO_2(e^-) + H_2O_2 \rightarrow TiO_2 + OH^{\bullet} + OH^- \quad (7)$$

$$Fe^{3+} + e^- \rightarrow Fe^{2+} \quad (8)$$

$$Fe^{2+} + H_2O_2 \rightarrow Fe^{3+} + OH^{\bullet} + OH \quad (9)$$

$$Fe^{2+} + O^{2-} \rightarrow Fe^{3+} + {O_2}^{2-} \quad (10)$$

$$Fe^{3+}(OH)^{2+} + h\upsilon \rightarrow Fe^{2+} + OH^{\bullet} \quad (11)$$

Metal ions in the sea sediment at the desired calcination temperature have modified the nature of the electrons and cavities produced in the conduction and capacity band of the photocatalyst. This has led to the efficiency of the photocatalyst in the removal of cephalexin. Therefore, these results clearly show that the electron correction of the titanium oxide is carried out by the metal ions present in the sea sediment by the strong and prolonged interaction between them [56]. The cavities, electrons, and vacuum results of the $OH^{\bullet}$ radical indicate that this radical play a very important role in the degradation of cephalexin [57]. In the ultrasound tool, hydroxyl radicals are produced by pyrolytic decomposition of water molecules, which are effective in mineralizing and removing pharmaceutical compounds. The incorporation of several advanced oxidation techniques (such as photolysis and sonolysis) increases the rate of degradation and mineralization resulting in a more economical large-scale process [27].

The efficiency of the photolytic process can be significantly increased when UV radiation is combined with H_2O_2. The oxidizing power of H_2O_2 can be improved by producing HO by O-O splitting with sufficient quantum photon energy (energy band > 213 kJ/mol at a wavelength < 280 nm). In systems containing UV/H_2O_2, the rate of degradation depends on the oxidant concentration. Concentrations above the optimum value have an inhibitory effect because the radicals tend to recombine and produce H_2O_2 [54].

In the system of 'sea sediment/titanate-UV- Ultrasound-H_2O_2', hydroxyl radicals are produced in large quantities in several ways simultaneously in the reactor. Thereby, increasing the degradation efficiency with the possibility of a reduction in purification time. Also, the electron-hole reconstitution in the photocatalyst is reduced by this coupling process, which further increases the degradation process efficiency. Electrons excited by iron and other metal ions in the system that block the electron reconstitution and the cavity are trapped [30]. It also reduces process costs due to the source of metal ions (readily available in sea sediment) coupled with the photocatalyst [7].

4. Conclusion

This study aimed to develop a new photocatalyst from sea sediment for cephalexin degradation. The sea sediment was modified with

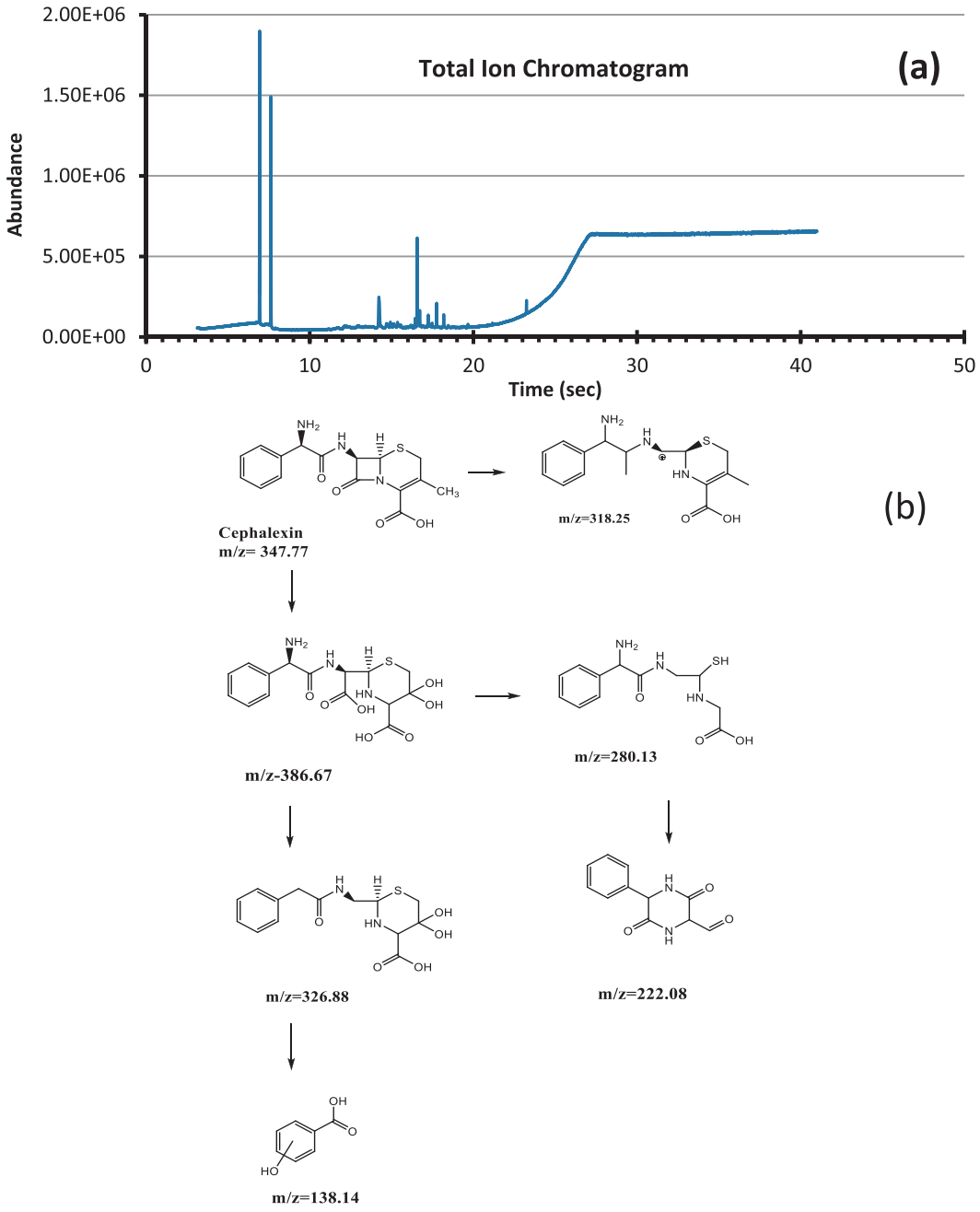

Fig. 9. (a) GC-mass graph for degradation of cephalexin by the developed system of "sea sediment/titanium-H_2O_2-UV-ultrasonic" (b) degradation path way of cephalexin.

titanium. Then, the effect of furnace temperature, duration time in the furnace, and the ratio of sea sediment to titanium was optimized in the term of the cephalexin removal. The catalyst was optimized at the furnace temperature of 500 ˚C, the furnace residence time of 2 h, and mL-titanate to the 2 g-sediment ratio of 12. The specifications were fully provided for the optimized photocatalyst. The optimum photocatalyst had a specific surface area of 52.29 m^2/g. The crystallite size of titanium oxide for the optimal photocatalyst was ~17.68 nm. The cephalexin removal efficiency of 94.71% was recorded by the 'sediment/TiO_2-UV-H_2O_2-ultrasonication' system. Also, the furnace temperature can affect the particle size and crystal structure of the generated samples. The optimal calcination time was 2 h. Calcination at or below the temperature of 500 ˚C resulted in lower photocatalytic activity. Less activity in very short calcination may be due to incomplete conversion of metal salts to the corresponding oxide in sediment. The stability and effectiveness of the catalyst depending on the total available pores and the solid bed surface in photocatalytic degradation. As the crystallite size decreases, the surface area increases that leading to an increase in the number of active sites on the catalyst activator surface, thereby enhancing the photovoltaic activity.

It can also be concluded that the photocatalysts prepared from sea sediment coated with different titanate loading do not have the same effect for the cephalexin removal. With increasing titanium content loaded on the sediments, due to higher surface area and higher photocatalytic activity, further removal of antibiotics resulted. It has also been shown that cephalexin antibiotic is broken down into simpler compounds that might be less toxic.

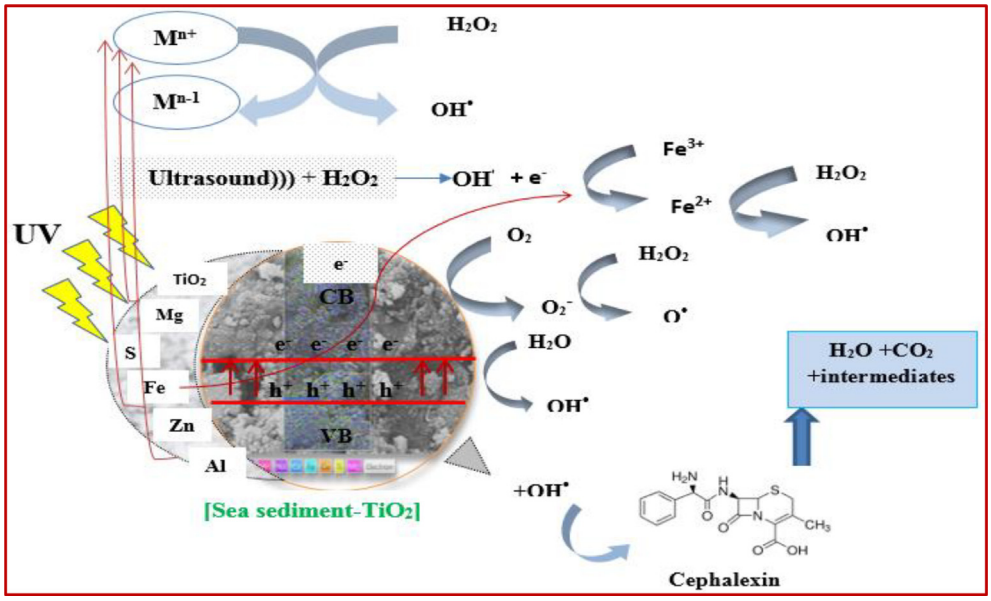

Fig. 10. Proposed mechanism of removal of cephalexin by the "sea sediment/titanium-H_2O_2-UV-ultrasonic" system.

CRediT authorship contribution statement

Fatemeh Tavasol: Formal analysis, Writing - original draft. **Taybeh Tabatabaie:** Methodology, Conceptualization. **Bahman Ramavandi:** Supervision, Writing - review & editing. **Fazel Amiri:** Software, Validation.

Declaration of Competing Interest

The authors declare that they have no known competing financial interests or personal relationships that could have appeared to influence the work reported in this paper.

Acknowledgements

This work was adapted from a Ph.D. dissertation in Environmental Engineering-Water& Wastewater approved in Islamic Azad University, Bushehr Branch, Bushehr. The authors of this research highly appreciate the support of Iran High-Tech Laboratory Network. The never-ending support of the Faculty of Health and Nutrition, Bushehr University of Medical Sciences is also highly praised.

Appendix A. Supplementary data

Supplementary data to this article can be found online at https://doi.org/10.1016/j.ultsonch.2020.105062.

References

[1] B. Petrie, R. Barden, B. Kasprzyk-Hordern, A review on emerging contaminants in wastewaters and the environment: Current knowledge, understudied areas and recommendations for future monitoring, Water Res. 72 (2015) 3–27.
[2] R. Kafaei, F. Papari, M. Seyedabadi, S. Sahebi, R. Tahmasebi, M. Ahmadi, G.A. Sorial, G. Asgari, B. Ramavandi, Occurrence, distribution, and potential sources of antibiotics pollution in the water-sediment of the northern coastline of the Persian Gulf, Iran, Sci. Total Environ. 627 (2018) 703–712.
[3] P. Bansal, A. Verma, C. Mehta, J. Singla, A.P. Toor, Assessment of integrated binary process by coupling photocatalysis and photo-Fenton for the removal of cephalexin from aqueous solution, J. Mater. Sci. 53 (2018) 7326–7343.
[4] C. Su, X. Lin, P. Zheng, Y. Chen, L. Zhao, Y. Liao, J. Liu, Effect of cephalexin after heterogeneous Fenton-like pretreatment on the performance of anaerobic granular sludge and activated sludge, Chemosphere 235 (2019) 84–95.
[5] S. Azimi, A. Nezamzadeh-Ejhieh, Enhanced activity of clinoptilolite-supported hybridized PbS–CdS semiconductors for the photocatalytic degradation of a mixture of tetracycline and cephalexin aqueous solution, J. Mol. Catal. A Chem. 408 (2015) 152–160.
[6] F. Torki, H. Faghihian, Sunlight-assisted decomposition of cephalexin by novel synthesized NiS-PPY-Fe_3O_4 nanophotocatalyst, J. Photoch. Photobiol. A 338 (2017) 49–59.
[7] P. Bansal, A. Verma, N, Ag co-doped TiO_2 mediated modified in-situ dual process (modified photocatalysis and photo-Fenton) in fixed-mode for the degradation of Cephalexin under solar irradiations, Chemosphere 212 (2018) 611–619.
[8] B. Kakavandi, N. Bahari, R. Rezaei Kalantary, E. Dehghani Fard, Enhanced sono-photocatalysis of tetracycline antibiotic using TiO_2 decorated on magnetic activated carbon (MAC@T) coupled with US and UV: A new hybrid system, Ultrason. Sonochem. 55 (2019) 75–85.
[9] Y. Zhao, S. Zhang, R. Shi, G.I.N. Waterhouse, J. Tang, T. Zhang, Two-dimensional photocatalyst design: A critical review of recent experimental and computational advances, Mater. Today (2019). Inpress.
[10] J. Kim, C.W. Lee, W. Choi, Platinized WO_3 as an environmental photocatalyst that generates OH radicals under visible light, Environ. Sci. Technol. 44 (2010) 6849–6854.
[11] H. Zangeneh, A.A.L. Zinatizadeh, M. Habibi, M. Akia, M. Hasnain Isa, Photocatalytic oxidation of organic dyes and pollutants in wastewater using different modified titanium dioxides: A comparative review, J. Ind. Eng. Chem. 26 (2015) 1–36.
[12] N. Raza, W. Raza, H. Gul, M. Azam, J. Lee, K. Vikrant, K.-H. Kim, Solar-light-active silver phosphate/titanium dioxide/silica heterostructures for photocatalytic removal of organic dye, J. Clean. Prod. 254 (2020) 120031.
[13] R. Asahi, T. Morikawa, H. Irie, T. Ohwaki, Nitrogen-doped titanium dioxide as visible-light-sensitive photocatalyst: Designs, developments, and prospects, Chem. Rev. 114 (2014) 9824–9852.
[14] J. Ananpattarachai, S. Seraphin, P. Kajitvichyanukul, Formation of hydroxyl radicals and kinetic study of 2-chlorophenol photocatalytic oxidation using C-doped TiO_2, N-doped TiO_2, and C, N Co-doped Ti_O2 under visible light, Environ. Sci. Poll. Res. 23 (2016) 3884–3896.
[15] M. Ksibi, S. Rossignol, J.M. Tatibouët, C. Trapalis, Synthesis and solid characterization of nitrogen and sulfur-doped TiO_2 photocatalysts active under near visible light, Mater. Lett. 62 (2008) 4204–4206.
[16] L. Li, Y. Yang, X. Liu, R. Fan, Y. Shi, S. Li, L. Zhang, X. Fan, P. Tang, R. Xu, W. Zhang, Y. Wang, L. Ma, A direct synthesis of B-doped TiO_2 and its photocatalytic performance on degradation of RhB, Appl. Surf. Sci. 265 (2013) 36–40.
[17] J. Zhang, Y. Huang, Y. Dan, L. Jiang, P3HT/Ag/TiO_2 ternary photocatalyst with significantly enhanced activity under both visible light and ultraviolet irradiation, Appl. Surf. Sci. 488 (2019) 228–236.
[18] J. Lyu, Z. Zhou, Y. Wang, J. Li, Q. Li, Y. Zhang, X. Ma, J. Guan, X. Wei, Platinum-enhanced amorphous TiO_2 -filled mesoporous TiO_2 crystals for the photocatalytic mineralization of tetracycline hydrochloride, J. Hazard. Mater. 373 (2019) 278–284.
[19] N.K. Pal, C. Kryschi, Improved photocatalytic activity of gold decorated differently doped TiO_2 nanoparticles: A comparative study, Chemosphere 144 (2016) 1655–1664.
[20] A.A. Ismail, T.A. Kandiel, D.W. Bahnemann, Novel (and better?) titania-based photocatalysts: Brookite nanorods and mesoporous structures, J. Photoch. Photobiol. A 216 (2010) 183–193.
[21] D. Li, W. Shi, Recent developments in visible-light photocatalytic degradation of antibiotics, Chinese J. Catal. 37 (2016) 792–799.
[22] S. Carbonaro, M.N. Sugihara, T.J. Strathmann, Continuous-flow photocatalytic treatment of pharmaceutical micropollutants: Activity, inhibition, and deactivation

of TiO2 photocatalysts in wastewater effluent, Appl. Catal. B 129 (2013) 1–12.
[23] T. Kaur, A. Sraw, R.K. Wanchoo, A.P. Toor, Solar assisted degradation of carbendazim in water using clay beads immobilized with TiO_2 & Fe doped TiO_2, Solar Energy 162 (2018) 45–56.
[24] M. Brigante, M.E. Parolo, P.C. Schulz, M. Avena, Synthesis, characterization of mesoporous silica powders and application to antibiotic remotion from aqueous solution. Effect of supported Fe-oxide on the SiO_2 adsorption properties, Powder Technol. 253 (2014) 178–186.
[25] B. Rhouta, L. Bouna, F. Maury, F. Senocq, M.C. Lafont, A. Jada, M. Amjoud, L. Daoudi, Surfactant-modifications of Na+-beidellite for the preparation of TiO_2-Bd supported photocatalysts: I-organobeidellite precursor for nanocomposites, Appl. Clay Sci. 115 (2015) 260–265.
[26] N.H. Ince, Ultrasound-assisted advanced oxidation processes for water decontamination, Ultrason. Sonochem. 40 (2018) 97–103.
[27] D. Kanakaraju, B.D. Glass, M. Oelgemöller, Advanced oxidation process-mediated removal of pharmaceuticals from water: A review, J. Environ. Manage. 219 (2018) 189–207.
[28] B. Ramavandi, M. Jafarzadeh, S. Sahebi, Removal of phenol from hyper-saline wastewater using Cu/Mg/Al-chitosan- H_2O_2 in a fluidized catalytic bed reactor, React. Kinet. Mech. Cat. 111 (2014) 605–620.
[29] M. Pazda, J. Kumirska, P. Stepnowski, E. Mulkiewicz, Antibiotic resistance genes identified in wastewater treatment plant systems – A review, Sci. Total Environ. 697 (2019) 134023.
[30] X. Liu, Y. Liu, S. Lu, W. Guo, B. Xi, Performance and mechanism into TiO_2/Zeolite composites for sulfadiazine adsorption and photodegradation, Chem. Eng. J. 350 (2018) 131–147.
[31] J. Gou, Q. Ma, X. Deng, Y. Cui, H. Zhang, X. Cheng, X. Li, M. Xie, Q. Cheng, Fabrication of Ag_2O/TiO_2-Zeolite composite and its enhanced solar light photocatalytic performance and mechanism for degradation of norfloxacin, Chem. Eng. J. 308 (2017) 818–826.
[32] A. Payan, A. Akbar Isari, N. Gholizade, Catalytic decomposition of sulfamethazine antibiotic and pharmaceutical wastewater using Cu- TiO_2@functionalized SWCNT ternary porous nanocomposite: Influential factors, mechanism, and pathway studies, Chem. Eng. J. 361 (2019) 1121–1141.
[33] Y.N. Kim, G.N. Shao, S.J. Jeon, S.M. Imran, P.B. Sarawade, H.T. Kim, Sol–gel synthesis of sodium silicate and titanium oxychloride based TiO_2–SiO_2 aerogels and their photocatalytic property under UV irradiation, Chem. Eng. J. 231 (2013) 502–511.
[34] M. Ramezanzadeh, M. Asghari, B. Ramezanzadeh, G. Bahlakeh, Fabrication of an efficient system for Zn ions removal from industrial wastewater based on graphene oxide nanosheets decorated with highly crystalline polyaniline nanofibers (GO-PANI): Experimental and ab initio quantum mechanics approaches, Chem. Eng. J. 337 (2018) 385–397.
[35] W. Zhang, L. Gai, Z. Li, H. Jiang, W. Ma, Low temperature hydrothermal synthesis of octahedral Fe_3O_4 microcrystals, J. Phys. D Appl. Phys. 41 (2008) 22.
[36] L. Lin, H. Wang, P. Xu, Immobilized TiO_2-reduced graphene oxide nanocomposites on optical fibers as high performance photocatalysts for degradation of pharmaceuticals, Chem. Eng. J. 310 (2017) 389–398.
[37] M. Li, Q. Liu, Z. Jia, X. Xu, Y. Shi, Y. Cheng, Y. Zheng, T. Xi, S. Wei, Electrophoretic deposition and electrochemical behavior of novel graphene oxide-hyaluronic acid-hydroxyapatite nanocomposite coatings, Appl. Surf. Sci. 284 (2013) 804–810.
[38] A.A. Javidparvar, R. Naderi, B. Ramezanzadeh, Epoxy-polyamide nanocomposite coating with graphene oxide as cerium nanocontainer generating effective dual active/barrier corrosion protection, Compos. B. Eng. 172 (2019) 363–375.
[39] X. Sun, R.-T. Guo, J. Liu, Z.-G. Fu, S.-W. Liu, W.-G. Pan, X. Shi, H. Qin, Z.-Y. Wang, X.-Y. Liu, The enhanced SCR performance of Mn/TiO_2 catalyst by Mo modification: Identification of the promotion mechanism, Int. J. Hydrogen. Energ. 43 (2018) 16038–16048.
[40] P.S. Pinto, G.D. Lanza, M.N. Souza, J.D. Ardisson, R.M. Lago, Surface restructuring of red mud to produce $FeO_x(OH)_y$ sites and mesopores for the efficient complexation/adsorption of β-lactam antibiotics, Environ. Sci. Poll. Res. 25 (2018) 6762–6771.
[41] M.D.G. de Luna, L.K.B. Paragas, R.-A. Doong, Insights into the rapid elimination of antibiotics from aqueous media by tunable C_3N_4 photocatalysts: Effects of dopant amount, co-existing ions and reactive oxygen species, Sci. Total Environ. 669 (2019) 1053–1061.
[42] S. Jagtap, K.R. Priolkar, Evaluation of ZnO nanoparticles and study of ZnO–TiO_2 composites for lead free humidity sensors, Sensor. Actuat. B-Chem. 183 (2013) 411–418.
[43] A. Mashayekh-Salehi, G. Moussavi, K. Yaghmaeian, Preparation, characterization and catalytic activity of a novel mesoporous nanocrystalline MgO nanoparticle for ozonation of acetaminophen as an emerging water contaminant, Chem. Eng. J. 310 (2017) 157–169.
[44] M. Rostamizadeh, F. Yaripour, Bifunctional and bimetallic Fe/ZSM-5 nanocatalysts for methanol to olefin reaction, Fuel 181 (2016) 537–546.
[45] M. Reli, K. Kočí, V. Matějka, P. Kovář, L. Obalová, Effect of calcination temperature and calcination time on the Kaolinite/TiO_2 composite for photocatalytic reduction of Co_2, GeoScie. Eng. 58 (2012) 10–22.
[46] B. Grzmil, B. Kic, M. Rabe, Inhibition of the anatase – Rutile phase transformation with addition of K_2O, P_2O_5, and Li_2O, Chem. Paper 58 (2004) 410–414.
[47] K. Zhang, F.J. Zhang, M.L. Chen, W.C. Oh, Comparison of catalytic activities for photocatalytic and sonocatalytic degradation of methylene blue in present of anatase TiO_2–CNT catalysts, Ultrason. Sonochem. 18 (2011) 765–772.
[48] M.A. Saepurahman, F.K. Abdullah, Chong, Dual-effects of adsorption and photodegradation of methylene blue by tungsten-loaded titanium dioxide, Chem. Eng. J. 158 (2010) 418–425.
[49] H. Zhao, S. Xu, J. Zhong, X. Bao, Kinetic study on the photo-catalytic degradation of pyridine in TiO_2 suspension systems, Catal. Today 93–95 (2004) 857–861.
[50] P. Bansal, A. Verma, Synergistic effect of dual process (photocatalysis and photo-Fenton) for the degradation of Cephalexin using TiO_2 immobilized novel clay beads with waste fly ash/foundry sand, J. Photoch. Photobiol. A 342 (2017) 131–142.
[51] M.A. Saepurahman, F.K. Abdullah, Chong, Preparation and characterization of tungsten-loaded titanium dioxide photocatalyst for enhanced dye degradation, J. Hazard. Mater. 176 (2010) 451–458.
[52] B. Neppolian, H. Jung, H. Choi, Photocatalytic degradation of 4-chlorophenol using TiO_2 and Pt-TiO_2 nanoparticles prepared by sol-gel method, J. Adv. Oxid. Technol. 10 (2007) 369–374.
[53] V.S. Antonin, J.M. Aquino, B.F. Silva, A.J. Silva, R.C. Rocha-Filho, Comparative study on the degradation of cephalexin by four electrochemical advanced oxidation processes: Evolution of oxidation intermediates and antimicrobial activity, Chem. Eng. J. 372 (2019) 1104–1112.
[54] J. He, Y. Zhang, Y. Guo, G. Rhodes, J. Yeom, H. Li, W. Zhang, Photocatalytic degradation of cephalexin by ZnO nanowires under simulated sunlight: Kinetics, influencing factors, and mechanisms, Environ. Int. 132 (2019) 105105.
[55] V.T. Gawande, K.G. Bothara, A.M. Marathe, Stress studies and identification of degradation products of cephalexin using LC–PDA and LC–MS/MS, Chromatographia 80 (2017) 1545–1552.
[56] M. Anpo, Applications of titanium oxide photocatalysts and unique second-generation TiO_2 photocatalysts able to operate under visible light irradiation for the reduction of environmental toxins on a global scale, in: A. Corma, F.V. Melo, S. Mendioroz, J.L.G. Fierro (Eds.), Studies in Surface Science and Catalysis, Elsevier, 2000, pp. 157–166.
[57] W. Lou, A. Kane, D. Wolbert, S. Rtimi, A.A. Assadi, Study of a photocatalytic process for removal of antibiotics from wastewater in a falling film photoreactor: Scavenger study and process intensification feasibility, Chem. Eng. Process 122 (2017) 213–221.